

# Intercomparison of methods for image quality characterization. II. Noise power spectrum<sup>a)</sup>

James T. Dobbins III

Duke Advanced Imaging Laboratories, Departments of Radiology and Biomedical Engineering, Duke University, Durham, North Carolina 27710

Ehsan Samei

Duke Advanced Imaging Laboratories, Departments of Radiology, Biomedical Engineering, and Physics, Duke University, Durham, North Carolina 27710

Nicole T. Ranger

Duke Advanced Imaging Laboratories, Department of Radiology, Duke University, Durham, North Carolina 27710

Ying Chen

Duke Advanced Imaging Laboratories, Departments of Radiology and Biomedical Engineering, Duke University, Durham, North Carolina 27710

(Received 8 April 2005; accepted for publication 17 February 2006; published 28 April 2006)

Second in a two-part series comparing measurement techniques for the assessment of basic image quality metrics in digital radiography, in this paper we focus on the measurement of the image noise power spectrum (NPS). Three methods were considered: (1) a method published by Dobbins *et al.* [Med. Phys. **22**, 1581–1593 (1995)], (2) a method published by Samei *et al.* [Med. Phys. **30**, 608–622 (2003)], and (3) a new method sanctioned by the International Electrotechnical Commission (IEC 62220-1, 2003), developed as part of an international standard for the measurement of detective quantum efficiency. In addition to an overall comparison of the estimated NPS between the three techniques, the following factors were also evaluated for their effect on the measured NPS: horizontal versus vertical directional dependence, the use of beam-limiting apertures, beam spectrum, and computational methods of NPS analysis, including the region-of-interest (ROI) size and the method of ROI normalization. Of these factors, none was found to demonstrate a substantial impact on the amplitude of the NPS estimates ( $\leq 3.1\%$  relative difference in NPS averaged over frequency, for each factor considered separately). Overall, the three methods agreed to within  $1.6\% \pm 0.8\%$  when averaged over frequencies  $> 0.15 \text{ mm}^{-1}$ . © 2006 American Association of Physicists in Medicine. [DOI: 10.1118/1.2188819]

Key words: Noise power spectrum (NPS), linear systems analysis, digital radiography, image quality, noise, IEC 62220-1

## I. INTRODUCTION

This paper is part of a two-part series comparing measurement methodologies for the modulation transfer function (MTF) and noise power spectrum (NPS). The NPS is one of the most common metrics describing the noise properties of imaging systems. The measurement of the NPS is conceptually straightforward but difficult to carry out experimentally, and there has not been universal agreement on the best methods for these measurements. Recently, there have been efforts by several bodies, including the AAPM<sup>1</sup> and the International Electrotechnical Commission (IEC),<sup>2</sup> to develop standards for these measurements. Despite the laudable effort to reach a consensus on the best measurement methodology, there is still a sizable literature of measurements made on various devices by a variety of methods.<sup>3–19</sup> Because of the variety of methods used, it is difficult to compare previously published NPS results using different methodologies. Therefore, there is a need for an intercomparison of these previously reported methods, as well as a comparison with the new IEC standard, so that investigators may know how to

interpret the results of different studies obtained using these various techniques. In this paper we describe a comparison of methods for a measurement of the NPS reported by Dobbins *et al.*<sup>3,20</sup> (hereafter, method A), Samei *et al.*<sup>4,5,14–17</sup> (hereafter, method B), and the IEC standard<sup>2</sup> (hereafter, method C). In a companion paper we report similar comparisons of methods for measuring the MTF.<sup>21</sup>

## II. BACKGROUND

The frequency-dependent NPS,  $NPS(f)$ , is defined as the variance per frequency bin of a stochastic signal in the spatial frequency domain. For a complete treatment of the derivation of the NPS formula, the interested reader is referred to another text.<sup>20</sup> Although it may be computed as the Fourier Transform of the autocovariance function by use of the Wiener-Kintchin Theorem,<sup>22</sup> the NPS is most commonly computed directly from the squared Fourier amplitude of two-dimensional image data using

$$\begin{aligned}
\text{NPS}(u_n, v_k) &= \lim_{N_x, N_y \rightarrow \infty} (N_x N_y \Delta x \Delta y) \langle |\text{FT}_{nk}[I(x, y) - \bar{I}]|^2 \rangle \\
&= \lim_{N_x, N_y \rightarrow \infty} \lim_{M \rightarrow \infty} \frac{N_x N_y \Delta x \Delta y}{M} \sum_{m=1}^M |\text{FT}_{nk}[I(x, y) - \bar{I}]|^2 \\
&= \lim_{N_x, N_y, M \rightarrow \infty} \frac{\Delta x \Delta y}{M \cdot N_x N_y} \sum_{m=1}^M \left| \sum_{i=1}^{N_x} \sum_{j=1}^{N_y} [I(x_i, y_j) - \bar{I}] e^{-2\pi i(u_n x_i + v_k y_j)} \right|^2, \tag{1}
\end{aligned}$$

where  $I(x_i, y_j)$  is the image intensity at the pixel location  $(x_i, y_j)$ ,  $\bar{I}$  is the global mean intensity,  $u$  and  $v$  are the spatial frequencies conjugate to  $x$  and  $y$ ,  $N_x$  and  $N_y$  are the numbers of pixels in the  $x$  and  $y$  directions of the digital image,  $\Delta x$  and  $\Delta y$  are the pixel spacings in the  $x$  and  $y$  directions, and  $M$  is the number of regions used for analysis in the ensemble average. Conventionally, the Fourier transform is normalized by dividing by  $N_x N_y$ .

The zero-frequency component is difficult to measure accurately, and is therefore almost always excluded from analysis. With that exclusion, the subtraction of the global mean in Eq. (1) may be eliminated, and thus only the squared Fourier amplitudes of raw noise data are considered.

Many factors influence the choice of methodology for measuring the NPS. Unfortunately, there is not a universal, standard method that will apply equally well to all situations, and some compromises are necessary, depending on the type of system being measured and the amount of data available. There are two principal difficulties in determining the best method for NPS analysis. The first such difficulty is that only a limited amount of data is available for analysis. The summations in the discrete Fourier transforms in Eq. (1) extend over an infinite spatial domain, but there is clearly not an infinite extent of data available for measurement. Also, the ensemble average in Eq. (1) requires an infinite number of samples to determine the true NPS, but again, an infinite amount of data is not available. Thus, some compromises must be made in order to get the “best” estimate of the NPS from the finite amount of available data. For two-dimensional image data, this compromise involves a trade-off between the size and number of the regions of interest (ROIs) used for analysis. A thorough treatment of the issues in selecting ROI size is beyond the scope of this paper, but another reference may be consulted for additional details.<sup>20</sup> In simplest terms, the size of the ROI should contain just enough pixels to adequately demonstrate the structure in the NPS curve. If the NPS curve is smoothly varying with frequency, then a very small ROI may be used; if there are spikes in the power spectrum, then the ROI must contain more pixels in order to have adequate sampling in frequency space so that the shape of the spikes is not adversely impacted. Some investigators have used data windowing (defined as the application of spatial weighting to image data) to further refine the resolution of NPS data in frequency space. Data windowing was not used with one of the methods de-

scribed in this paper (method A in which all pixels analyzed had the same weighting), but a Hamming window was used on the data for the other two analysis approaches (methods B and C).

The second difficulty in making accurate NPS measurements is that practical data contains some static artifactual components in addition to the stochastic noise that one desires to measure. This artifactual structure may manifest itself as background shading due to the heel effect or inverse square exposure variation, or as a fixed pattern due to the structure in the detector. It is almost always desirable to remove shading artifacts because these contribute to the squared Fourier components at low frequency, but do not represent stochastic noise. Various approaches are used in this paper to eliminate background shading artifacts, depending on the NPS measurement method being used. Fixed pattern noise should not be removed from the image used to compute NPS if the noise is spatially stochastic (even though temporally constant), because it contributes to the noise pattern in a given image, hampering an observer’s ability to discern the desired signal from noise. The flat-panel detector used for the NPS measurements in this paper does a gain and offset correction that inherently eliminates a large amount of the stochastic fixed pattern noise; however, a small amount remains, particularly at low frequencies. A subtraction method can be used to determine the amount of residual fixed pattern noise in the NPS.

It is important when evaluating the NPS on a given device to consider the entire two-dimensional NPS. There can be spikes or other noise artifacts that do not show up adequately if a simple one-dimensional plot is examined.<sup>3</sup> However, due to the number of intercomparisons in this paper, and due to the fact that the detector being used for measurement has no discernable off-axis noise artifacts, only one-dimensional plots will be presented here. In order to improve the standard error of one-dimensional NPS curves, it is customary to average data from a thick band through two-dimensional frequency space near the axes; methods described herein differ as to whether the on-axis data is included in those averages, and such differences will be noted.

### III. METHODS

The three NPS methods compared in this article differ in various acquisition and processing parameters [beam quality, ROI size, configuration and number of ROIs, background

TABLE I. Standard parameters for the NPS methods evaluated. Methods A, B, and C represent methods published by Dobbins *et al.* (Refs. 3 and 20), Samei *et al.* (Refs. 4, 5, and 14–17), and the IEC (Ref. 2), respectively. Method B has historical and current versions differing by the number of ROIs used. The beam spectrum for method C was set at a 70 kV nominally, with kilovoltage adjusted to give a HVL of 7.1 mm Al according to the IEC procedure for the RQA5 beam quality. ROIs were either in overlapping (OL) or nonoverlapping (NOL) patterns. For detrending, method A used a 2-D first-order fit to the data within a ROI, while methods B and C used a 2-D second-order polynomial fit to ROI data. Data rows averaged indicate how many adjacent rows of data in the two-dimensional NPS were averaged to give the one-dimensional NPS plot. Method B included the data along the axis in the two-dimensional NPS, whereas methods A and C excluded the on-axis data. Methods A and B used no external beam apertures, but method C included IEC-specified external beam apertures.

Method	kV	Filtration	# ROIs	ROI size	Detrending	Data rows averaged
Method A	70	0.5 mm Cu	64 NOL	128 × 128	2-D (first order)	8 (w/o axis)
Method B (historical)	70	19 mm Al	100 NOL	128 × 128	2-D (second order)	15 (w/ axis)
Method B (current)	70	19 mm Al	343 OL	128 × 128	2-D (second order)	15 (w/ axis)
Method C	74	21 mm Al	160 OL	256 × 256	2-D (second order)	14 (w/o axis)

detrending, and methods of extracting one-dimensional (1-D) NPS data from the 2-D NPS]. Table I lists the standard acquisition and processing parameters associated with these three methods. In addition to comparing the three methods directly, a number of subcomparisons were performed to elucidate the influence of the various parameter choices associated with NPS methodology. Table II lists the combinations of parameters for image acquisition and analysis for each of the sub-comparison evaluations performed. In the following

sections we describe the details of the imaging system, beam conditions, image acquisition, and the NPS processing employed in this study.

### A. Imaging system

A commercial-grade *a*:Si/CsI flat-panel radiographic detector (equivalent to that in the Revolution XQ/i system, GE Healthcare, Milwaukee, WI) was used for all measurements.

TABLE II. Acquisition and processing parameters for each measurement condition evaluated. Beam spectra: Method A (70 kV, 0.5 mm Cu), method B (70 kV, 19 mm Al), and method C (IEC RQA5, 74 kV, 21 mm Al).

Beam spectrum	Analysis method	Apertures	No. images	No. indep. image pixels	Analysis area	ROI size	Overlapping vs nonoverlapping
C	C	External (per IEC)	1	409 600	640 × 640	256	OL
			3	1 228 800			
			10	4 096 000			
C	C	External (per IEC)	1	262 144	512 × 512	256	NOL
			3	786 432			
			10	2 621 440			
C	C	None	3	1 228 800	640 × 640	256	OL
			10	4 096 000			
C	A	External (per IEC)	10	4 096 000	640 × 640	128	NOL
C	B (Historical)	External (per IEC)	10	4 096 000	640 × 640	128	NOL
C	B (Current)	External (per IEC)	3	1 228 800	640 × 640	128	OL
A	A	None	1	1 048 576	1024 × 1024	128	NOL
A	C	None	3	1 228 800	640 × 640	256	OL
B	B (Historical)	None	1	1 638 400 <sup>a</sup>	1280 × 1280 <sup>a</sup>	128	NOL
B	B (Current)	None	1	1 638 400 <sup>a</sup>	1280 × 1280 <sup>a</sup>	128	OL
B	C	None	3	1 228 800	640 × 640	256	OL

<sup>a</sup>Previously published historical analysis areas were 1664 × 1664 (2 768 896 pixels) NOL and 1728 × 1728 (2,985,984 pixels) OL; current evaluation area was modified due to limited field of view as a result of the ionization detector placement.

The detector, with a 0.2 mm pixel pitch and a  $41 \times 41$  cm<sup>2</sup> overall field of view, was mounted in a prototype research radiographic system and was coupled to a standard x-ray tube and generator. The antiscatter grid, system faceplate, and automatic exposure control sensors were removed for all measurements, in keeping with the IEC standard. The details of the detector calibration performed prior to acquisition of imaging data are outlined in a concurrent paper.<sup>21</sup> As the intent of this paper was not to characterize the NPS performance of a specific device *per se*, but rather to identify the way in which three NPS measurement methods compare, the choice of detector used for these measurements was not critical. However, in order to make this intercomparison of methods as generalizable as possible, the imaging system used was selected as representative of contemporary digital radiographic systems.

## B. Beam conditions

The three NPS methods compared in this paper all used roughly comparable beam spectra (70 kV nominal with added filtration). Method A used 70 kV with 0.5 mm Cu filtration; method B used 70 kV with 19 mm Al filtration; and method C used 74 kV (70 kV nominal) with 21 mm Al filtration. Spectra for each method matched those reported in previous publications. Method C (the IEC method) specified an initial Al filtration and a given half-value layer (HVL) rather than a specific tube kilovoltage. The kilovoltage for method C was thus adjusted to 74 kV to achieve an IEC-specified HVL of 7.1 mm Al with a 21 mm added Al filter. Measured HVLs of the 70 kV beams for methods A and B were 6.7 and 6.6 mm Al, respectively. Further details of the beam conditions are provided in a concurrent paper.<sup>21</sup>

## C. System response function

System response functions were measured for the spectra of methods A, B, and C to verify detector linearity and to determine the exposure associated with each NPS estimate. The method of measuring response curves is described in detail in a companion paper.<sup>21</sup> Briefly, response curves were generated by acquiring flat-field images for each of the three spectra over a range of mAs settings. Mean pixel values were determined in a  $100 \times 100$  pixel region near the center of each image. Exposure values were measured with a narrow-beam geometry using a calibrated ion chamber (MDH Model 1015, 10X5-6 ionization chamber, Radcal, Monrovia, CA) placed 90.5 cm from the focal spot with the detector moved vertically out of the beam field of view (i.e., exposure measured free in air with no backscatter from the detector). Exposure values at the plane of the detector were then computed by using the inverse square law. For each beam quality, a linear fit to the mean pixel value versus exposure was used to estimate exposure in the flat-field images used for the NPS estimation.

## D. Image acquisition

For all measurements, flat-field images were acquired with nothing in the beam but the required filtration (and IEC-specified apertures, where indicated). The filtration was placed on the exit side of the collimator. The focal spot to detector distance was 184.5 cm. Method C measurements were made with apertures, in keeping with the IEC standard (illustrated in Fig. 1 of a concurrent paper<sup>21</sup>) and without apertures for comparison purposes. For Methods A and B, no apertures were used, but the beam was collimated to just beyond the edge of the detector panel.

Images were acquired for the different spectra at various levels of incident exposure. The IEC standard specifies that exposures of approximately  $E_{nl}/3.2$ ,  $E_{nl}$ , and  $3.2E_{nl}$  be used, where  $E_{nl}$  is the "normal level" exposure for a particular imaging application for a given device. In consultation with the manufacturer of the flat-panel device, a value  $E_{nl}$  of approximately 0.4 mR ( $3.5 \mu\text{Gy}$ ) was used. Three images were acquired for the beam spectra of methods A and B and ten images for method C (based on the IEC requirement to use 4 000 000 independent measurement pixels).

To minimize detector lag effects, a minimum interval of 2 min was employed between image acquisitions in a progression from low to high exposures and from open field of view to a restricted field of view. A minimum interval of 10 min was used between aperture configurations. All NPS data acquisitions were completed within 24 h of the detector calibration.

## E. NPS processing

The flat-field image data were processed using the NPS processing methods specified by methods A, B, and C. The methods differed in terms of various parametric choices and algorithmic implementations. Among those, the number, size, and overlapping of the ROIs varied by measurement method (Table II). Method A used ROIs of size  $128 \times 128$  pixels; 64 such nonoverlapping ROIs were used in a  $1024 \times 1024$  region near the center of the image, in keeping with the previously published results with this method. Two configurations were used for method B: the B-historical method used nonoverlapping  $128 \times 128$  ROIs and the B-current method used overlapping ROIs of the same size, reflecting a modification of method B over time. (Historically, method B used a total area of  $1664 \times 1664$  pixels for analysis, but in these experiments the total area of analysis was restricted to  $1280 \times 1280$  due to the placement of the ion chamber). For method C, ROIs of size  $256 \times 256$  were used in a  $640 \times 640$  pixel region near the center of each image; the ROIs were arranged in four different overlapping patterns, each pattern offset by one-half the ROI size in each dimension, in keeping with the IEC standard, giving a total of 16 overlapped ROIs per image. In this arrangement, 16% of pixels appeared in only one ROI, 48% appeared in two ROIs, and 36% appeared in four ROIs. Other combinations of ROI size and overlapped/nonoverlapped orientation were used for certain specific data analyses in order to elucidate effects due to the ROI size and the number of ROIs.

The methods also differed in terms of detrending techniques. Each method used a detrending technique to correct for possible background gradients in individual ROIs. For method A, a two-dimensional first-order fit (i.e., planar ramp) was subtracted from the data prior to NPS analysis. It should be noted that because method A excludes data on the  $u$  and  $v$  axes when generating the one-dimensional NPS plots, this subtraction does not change the measured one-dimensional curves, as a ramp subtraction only affects the data on the frequency axes. Method B employed a quadratic (2-D second-order polynomial) surface fit to the data in each ROI and then subtracted that surface prior to NPS analysis. For method C, the same NPS detrending technique used for method B was also employed, satisfying all requirements of the IEC standard.

In addition to detrending individual ROIs, the methods also included the means to correct for small regional variation in exposure from ROI to ROI. Such regional variations are often caused by the heel and inverse square law effects across the detector's field of view. Correcting for these variations provides an estimate of NPS that is less biased by such regional exposure variations. For all three methods, the correction involved normalizing the pixel values in each ROI by a function of the ROI mean relative to some reference mean. Method A normalized the pixel values in each ROI by the ratio of the square root of the ROI mean to the global mean. Methods B and C normalized pixel values in each ROI by the ratio of ROI mean to the mean of a reference ROI (located in the upper left corner of the image). The effect of the normalization procedure was determined by comparing NPS estimates with both of these approaches to normalization.

The NPS is often used as an input to the computation of detective quantum efficiency (DQE). In the DQE computation, it is necessary to correct for the gain of the system, and the NPS (given in units of digital value squared times  $\text{mm}^2$ ) is divided by the square of the mean value of the pixels used for analysis (in units of digital value). This ratio is referred to as the normalized noise power spectrum (NNPS), and has units of  $\text{mm}^2$ :

$$\text{NNPS}(u,v) = \frac{\text{NPS}(u,v)}{(\text{large area signal})^2}. \quad (2)$$

This ratio assumes that the pixel values have been linearized with respect to exposure. Because the NNPS has been historically reported in earlier work by Dobbins *et al.* and Samei *et al.*, it was used as the basis of the results reported in this paper. It should be noted that in the literature, the terms "NPS" and "NNPS" are often used interchangeably to refer to the normalized noise power spectrum.

The Fourier transform used for method A was a FFT adapted from the method of Bracewell,<sup>23</sup> and hand-coded by the author. The FFT used for the data analysis with methods B and C was hand coded and adapted from the work of Brigham.<sup>24</sup> For method A, 4 lines of data just above and 4 lines just below the  $u$ -axis in the  $128 \times 128$  two-dimensional NPS space were used to generate the one-dimensional NPS curves, with the on-axis data excluded. For each datum in

this 8-row set, the radial frequency given by  $\sqrt{(u^2+v^2)}$  was used; all data in this 8-row set were then averaged into bins of interval  $0.05 \text{ mm}^{-1}$ . The result was an approximation of the one-dimensional NPS along the direction of the  $u$  axis from a band through the two-dimensional NPS space. For method B, data were similarly processed, but a total of 15 rows (7 rows above and 7 below, including the on-axis row) was used to determine an approximation of the one-dimensional NPS along the direction of the  $u$  axis. Method C used a total of 14 rows (7 rows above and 7 below, excluding the on-axis row). For methods B and C, data were also averaged into bins of interval  $0.05 \text{ mm}^{-1}$ . A subsequent analysis of data along the  $v$  axis for one measurement condition found essentially no difference between the  $u$ - and  $v$ -axis directions; therefore, only the  $u$ -axis data were processed for the remaining measurements.

## IV. RESULTS

Results are described in this section for each subcomparison performed as well as for an overall comparison of methods A, B, and C.

### A. Precision of NPS estimate

The NPS defined in Eq. (1) is an ensemble average over an infinite number of noise realizations; for a finite number of noise realizations, there will be an uncertainty associated with the NPS estimate. The standard deviation of an NPS estimate is proportional to the NPS; therefore, the relative uncertainty (i.e., the coefficient of variation) of NPS estimates is independent of frequency. This uncertainty has been shown by Wagner and Sandrik<sup>25</sup> to vary as  $1/\sqrt{N}$ , where  $N$  is the number of independent frequency bin measurements associated with a given NPS value. As a validation of the predicted uncertainty values, we measured the relative uncertainty in NNPS using the method A processing technique with  $25, 128 \times 128$  nonoverlapping ROIs and 8 rows of data averaged, and found it to be  $6.48\% \pm 0.25\%$ ; this value agreed well with the value of  $6.25\%$  predicted by Wagner and Sandrik.

In the case of overlapping ROIs, the uncertainty in the ensemble average does not decrease as the square root of the number of ROIs, because the overlapping ROIs do not contain statistically independent data. To determine the relative uncertainty between overlapping and nonoverlapping ROIs, we measured the relative uncertainty using the method C processing technique with  $256 \times 256$  ROIs and 14 rows of data averaged in configurations of 4 nonoverlapping or 16 overlapping ROIs per image. When no Hamming window was used, the relative uncertainty, averaged over all frequencies, in the overlapping ROI case relative to the nonoverlapping ROI case had a ratio of 0.80, which is equal to the square root of the reciprocal number of independent pixels in the two cases. When the Hamming window was used, the relative uncertainty in both the overlapping and nonoverlapping ROI cases was worse, although the uncertainty in the overlapping case relative to the nonoverlapping case differed by a greater amount (a ratio of 0.54). This larger difference

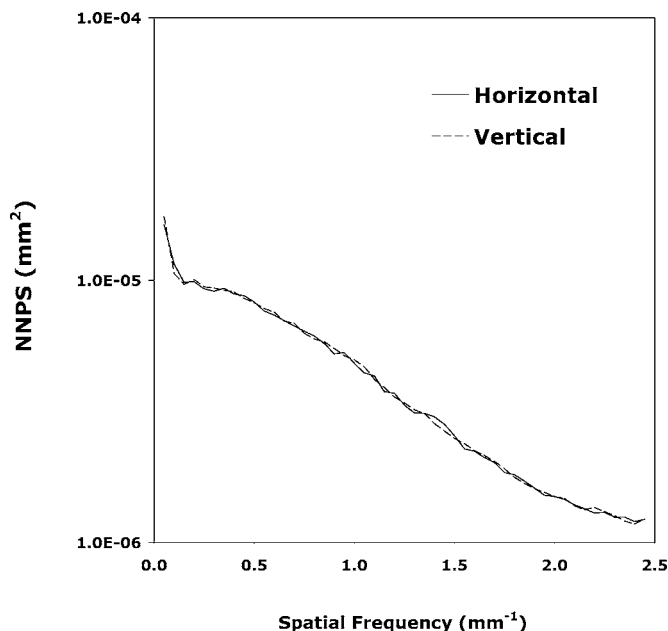


FIG. 1. NNPS directional dependence. Method C spectrum (IEC RQA5, 74 kV, 21 mm Al filtration) with apertures. Incident exposure was 0.53 mR. Ten images used for analysis with 160 total overlapping ROIs of size  $256 \times 256$ , using the method C analysis procedure. Error bars:  $\pm 2.3\%$ .

between overlapping and nonoverlapping ROIs with the Hamming window is likely due to the better statistical independence of values in the overlapping ROIs resulting from nonuniform pixel weighting introduced by the Hamming window.

The factors relating to overlapping ROIs and a Hamming window were used to adjust the relative uncertainty predicted by the method of Wagner and Sandrik for all subsequent data reported below.

## B. Directional dependence

Figure 1 depicts the directional dependence of the measured NNPS in the horizontal and vertical directions for one of the measurement conditions. The method C (IEC) spectrum with apertures was used, at an incident exposure of 0.53 mR. The average NNPS estimate from ten images was computed using method C data analysis procedures, with overlapping ROIs of size  $256 \times 256$ . The two curves were virtually identical (0.3% relative difference between curves, averaged over all frequencies; estimated standard error of average:  $\pm 0.5\%$ ) with no discernable trend of the difference between curves, and hence only horizontal data are reported for the remainder of the graphs.

## C. Impact of beam quality

The effect of beam spectrum is shown in Fig. 2 for the spectra of methods A–C (without apertures). Because the mean exposure in each case is slightly different, the product of exposure and normalized noise power ( $E^* \text{NNPS}$ ) is plotted in order to produce a quantity that in the absence of additive noise is independent of incident exposure, and there-

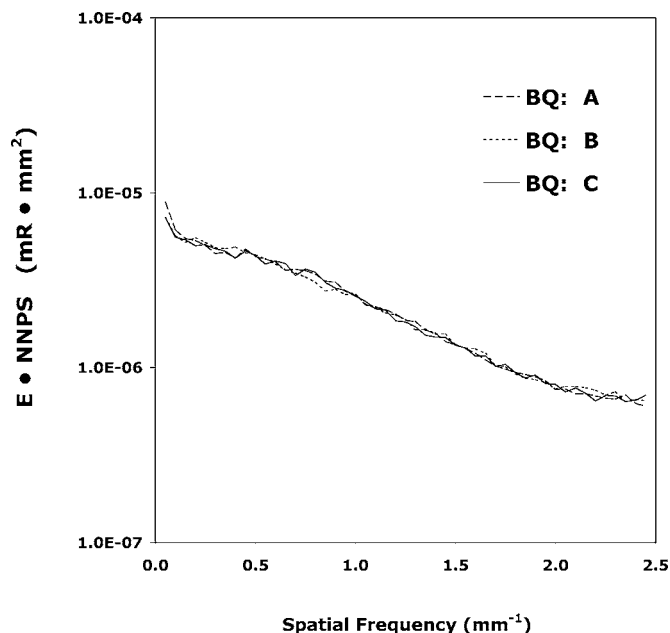


FIG. 2. NNPS dependence on beam spectrum. Plotted is incident exposure times NNPS for method A spectrum (70 kV, 0.5 mm Cu filtration), method B spectrum (70 kV, 19 mm Al filtration), and method C spectrum (IEC RQA5, 74 kV, 21 mm Al filtration), all without apertures. Incident exposures were 0.49 mR (A), 0.40 mR (B), and 0.43 mR (C, no apertures). Three images used for analysis with 48 total overlapping ROIs of size  $256 \times 256$ , using method C (IEC) analysis procedure. Error bars:  $\pm 4.2\%$ . BQ=beam quality.

fore, more easily compared across spectra.<sup>10</sup> The incident exposures ( $E$ ) were 0.49, 0.40, and 0.43 mR for the spectra of methods A, B, and C (without apertures), respectively. The average NNPS estimate from three images was computed for each case, using the method C data analysis procedure and overlapping ROIs of size  $256 \times 256$ . The  $E^* \text{NNPS}$  data demonstrated very little dependence on the spectrum ( $\leq 0.9\%$  relative difference between curves, averaged over all frequencies; estimated standard error of average:  $\pm 0.8\%$ ).

## D. Impact of beam limitation

The impact of including the IEC-required apertures in the method C measurement procedure is demonstrated in Fig. 3. The method C spectrum and analysis technique were used in both cases. The product of exposure and normalized noise power is plotted. Incident exposures were 0.53 and 0.56 mR for the images with and without apertures, respectively. The average NNPS estimate from ten images was computed for each case, using overlapping ROIs of size  $256 \times 256$ . Little difference was noted between the  $E^* \text{NNPS}$  measured with and without apertures (2.3% relative difference between curves, averaged over all frequencies; estimated standard error of average:  $\pm 0.5\%$ ).

## E. Impact of analysis method

The effect of the noise power analysis method, independent of spectrum, is shown in Fig. 4. The same beam condition was used for all curves (method C spectrum, with aper-

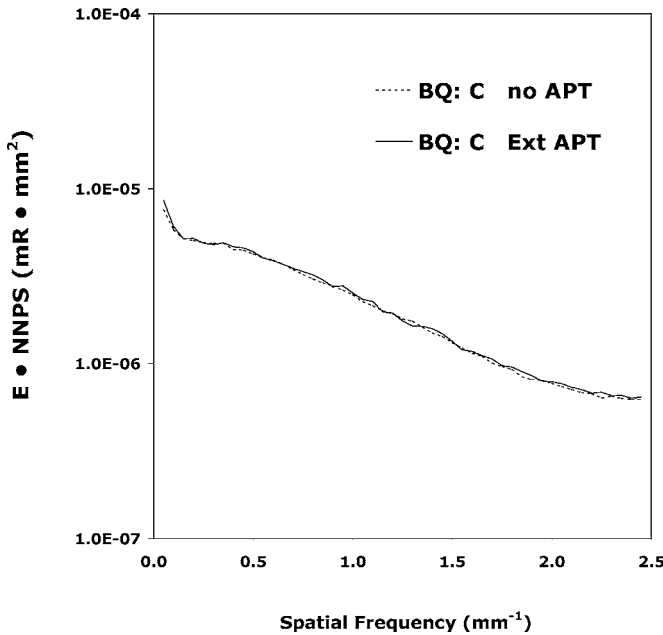


FIG. 3. NNPS dependence on IEC-specified apertures with method C (IEC) spectrum. Incident exposures were 0.53 mR (with apertures—Ext APT) and 0.56 mR (without apertures—no APT). Ten images used for an analysis with 160 total overlapping ROIs of size 256×256, using method C analysis procedure. Error bars: ±2.3%. BQ=beam quality.

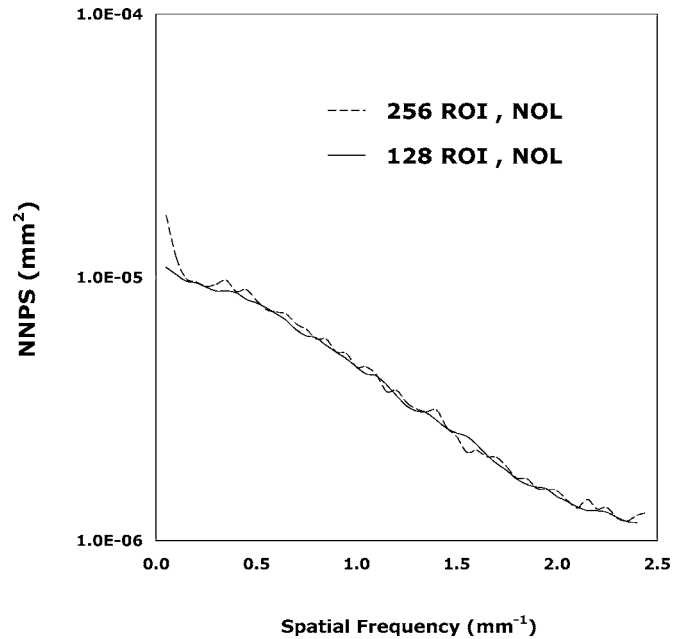


FIG. 5. NNPS dependence on ROI size using the method C spectrum with apertures. Ten images used for analysis. ROIs used were 160 total nonoverlapping (NOL) ROIs of size 128×128 and 40 total nonoverlapping ROIs of size 256×256, both using the method C analysis procedure. Error bars: <±4.3%.

tures), but with four different methods of analysis, as specified by methods A, B-historical, B-current, and C. A different number of images was used for the four methods in order to maintain approximately equivalent statistics (ten images for methods A and B-historical; three images for meth-

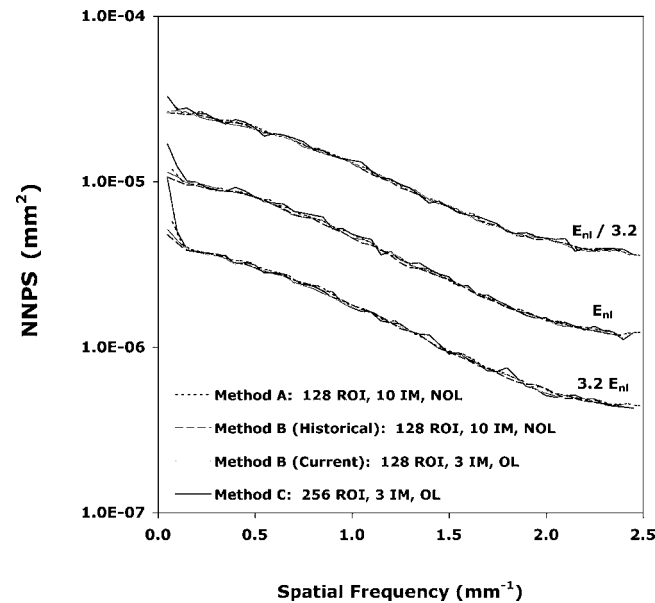


FIG. 4. NNPS dependence on analysis method. “Normal level” exposure ( $E_{nI}$ ) is approximately 0.4 mR. Method C spectrum with apertures. ROIs used were 250 total nonoverlapping (NOL) ROIs of size 128×128 (A), 250 total nonoverlapping ROIs of size 128×128 (B-historical), 219 total overlapping (OL) ROIs of size 128×128 (B-current), and 48 total overlapping ROIs of size 256×256 (C). IM indicates the number of images used. Error bars: <±4.2%.

ods B-current and C). The average NNPS estimate from these images was computed in each case. The ROI sizes for the four methods were 128×128 nonoverlapped ROIs for methods A and B-historical, 128×128 overlapped ROIs for method B-current, and 256×256 overlapped ROIs for method C. Data are shown for the three exposure levels specified by the IEC (method C). There was only a small difference in the NNPS estimates produced by the four analysis methods for frequencies >0.15 mm<sup>-1</sup>. For example, at the middle exposure there was a ≤3.1% relative difference between curves, averaged over all frequencies above 0.15 mm<sup>-1</sup> (estimated standard error of average <±0.8%). The differences were slightly lower when comparing only between methods A and B (≤1.2% average relative difference between curves, averaged over all frequencies above 0.15 mm<sup>-1</sup>).

**F. Impact of ROI size**

Figure 5 shows the dependence of the NNPS on the ROI size used for analysis. Nonoverlapping ROIs of size 128×128 and 256×256 were used, with data taken from a 512×512 region near the center of the image in both cases. The method C spectrum (IEC RQA5, 74 kV, 21 mm Al) with apertures and Method C analysis technique were used. Fourteen rows of data in the two-dimensional NNPS were averaged (excluding the axis) for both the 128×128 and 256×256 size ROIs. Ten images were used for an analysis of both ROI sizes, and the NNPS results from the ten images averaged. For the smoothly varying NNPS curves obtained in these experiments, there was very little difference in the NNPS estimate with either ROI size (1.8% relative differ-

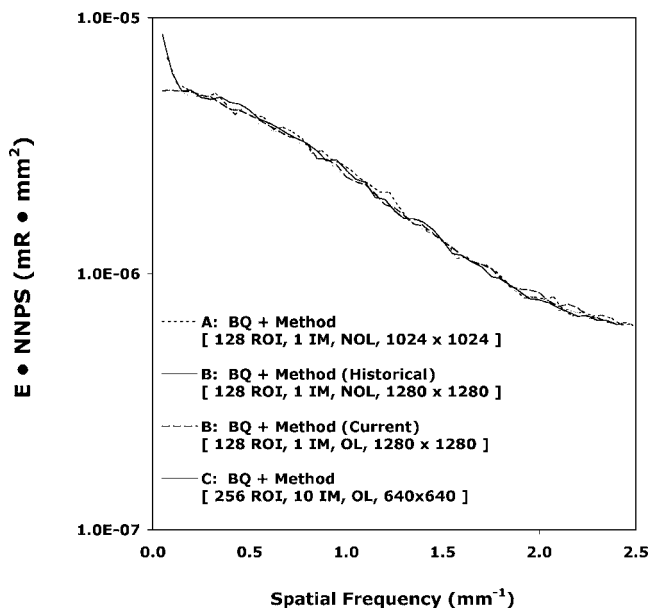


FIG. 6. Overall comparison of NNPS methods. Plotted is the incident exposure times NNPS for the method A spectrum (70 kV, 0.5 mm Cu filtration), method B spectrum (70 kV, 19 mm Al filtration), and the method C spectrum (IEC RQA5, 74 kV, 21 mm Al, with apertures). Incident exposures were 0.49 mR (A), 0.40 mR (B), and 0.53 mR (C, with apertures). ROIs used were 64 nonoverlapping ROIs of size  $128 \times 128$  (A), 100 nonoverlapping ROIs of size  $128 \times 128$  (B-historical), 343 overlapping ROIs of size  $128 \times 128$  (B-current), and 160 total overlapping ROIs of size  $256 \times 256$  (C). IM indicates the number of images used for analysis. BQ=beam quality. Error bars:  $\leq \pm 3.9\%$ .

ence between curves, averaged over all frequencies; estimated standard error of average  $< \pm 0.9\%$ ). In this particular case, the larger ROI size demonstrated worse precision of measurement; however, if the number of data rows analyzed were adjusted for ROI size, such that comparable areas in the two-dimensional NNPS were used for analysis, then the identical precision of measurement would be found for both ROI sizes.

### G. Overall comparison of methods

Figure 6 shows the final overall comparison of methods A, B, and C, including all components of the differences between the methods (each used its own historical ROI size, spectrum, number of acquired images, and analysis method). The exposure conditions used were 70 kV with 0.5 mm Cu (no apertures) for method A; 70 kV with 19 mm Al (no apertures) for method B; and 74 kV with 21 mm Al (with apertures) for method C. ROI conditions were the following: 1 image using 64 nonoverlapping ROIs of size  $128 \times 128$  for method A; 1 image using 100 nonoverlapping ROIs of size  $128 \times 128$  for method B-historical; 1 image using 343 overlapping ROIs of size  $128 \times 128$  for method B-current; and 10 images using 160 overlapping  $256 \times 256$  ROIs (16 per image) for method C. The data is plotted in terms of the product of exposure and NNPS in order to account for the impact of minor differences in incident exposure in each case. There were very small differences between the four curves above

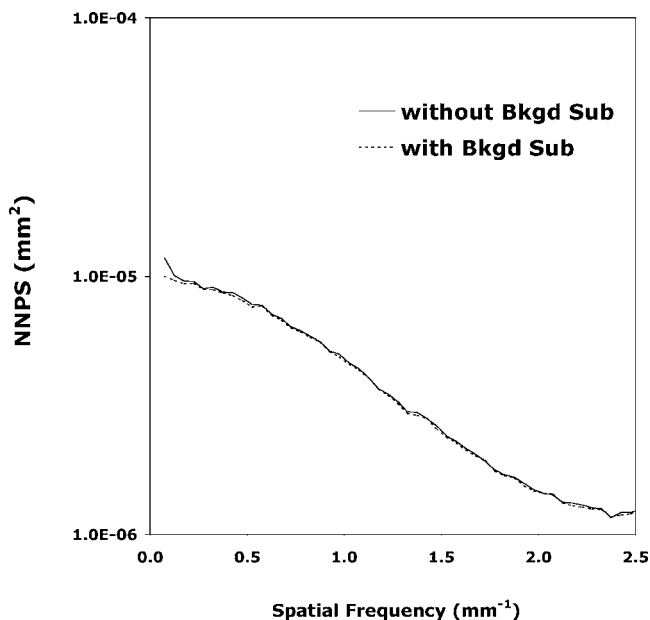


FIG. 7. Impact of background subtraction on the NNPS. Method C spectrum (IEC RQA5 74 kV, 21 mm Al filtration) with apertures at an incident exposure of 0.53 mR. Ten images were used for the analysis with 250 total nonoverlapping ROIs of size  $128 \times 128$ , using the method A analysis procedure. A fixed background was determined as the mean of the ten images, subsequently subtracted from original images. The NNPS was computed with and without background subtraction.

$0.15 \text{ mm}^{-1}$  ( $\leq 1.6\%$  relative difference between curves, averaged over all frequencies above  $0.15 \text{ mm}^{-1}$ ; estimated standard error of average  $< \pm 0.8\%$ ).

### H. Influence of fixed pattern noise

All of the NNPS data depicted above include the effects of fixed patterns in the images in addition to the stochastic components from the x-ray flux and electronic noise. The fixed patterns that are stochastic (such as from random spatial variation in the detector response) should be included in the total NPS. However, as indicated earlier, a flat image may contain fixed patterns that are artifactual and not stochastic. In order to gain an appreciation for the amplitude of the fixed pattern components in the NPS estimates, an average of 10 flat-field images was performed and subtracted from each image to yield a set of images with the suppression of spatially fixed patterns common to all. Figure 7 demonstrates the relationship between the subtracted and the unsubtracted NNPS estimates using method A on the IEC beam spectrum (with apertures). It can be seen that the subtracted and unsubtracted NNPS estimates are virtually identical above about  $0.15 \text{ mm}^{-1}$ , indicating that the detector pixel-to-pixel gain correction adequately eliminates fixed pattern noise and any systematic effect in the NNPS estimate from nonstochastic patterns is only important at the very lowest spatial frequencies. This finding does not speak directly to the comparisons of the three NNPS methods, but demonstrates an important way of distinguishing systematic effects in the reported NNPS measurements.

## I. Impact of normalization technique

As noted earlier, an additional detail of evaluation relates to the technique used to correct for small variations in regional exposure. In method A, the mean of each ROI was measured and used to adjust the pixel values of each ROI by the square root of the ROI mean; this permitted a normalization of the NPS across ROIs for slight variations in regional exposure (such as from the heel effect). Methods B and C corrected the data in each ROI by the ROI mean, rather than the square root of the mean, with the intent of accomplishing the same goal. An evaluation of the difference due to the two normalization procedures was conducted on one image acquired with the method C spectrum at 0.53 mR. Method A analysis was performed using 25 nonoverlapping ROIs of size  $128 \times 128$ . The maximum difference between NNPS values at any given frequency for the two normalization methods was 0.02%. Therefore, it was concluded that differences in the method of normalization had a negligible effect on the measured NNPS.

## V. DISCUSSION

Overall, the NNPS estimates were comparable to previously obtained results<sup>7,16</sup> using the same detector. The NNPS curves demonstrated a very small additive noise component (manifested as a white noise pedestal) with a component associated with a  $\text{MTF}^2$  smoothly varying above about  $0.15 \text{ mm}^{-1}$ . The subtraction of the mean of ten images revealed that the systematic rise in the NNPS estimate for frequencies below  $<0.15 \text{ mm}^{-1}$  was likely due to fixed pattern features in the images uncorrected by the detector's pixel-by-pixel gain correction. For nonsubtraction methods, this low-frequency rise is typical of the NNPS curves reported in the literature.<sup>3,7</sup> The low-frequency rise was less with method B processing methods; these used a second-order detrending that suppressed the low-frequency rise in comparison to method A (which used first-order detrending) or method C (which also used a second-order polynomial fit but larger ROIs, and hence, worse detrending).

All of the various acquisition and processing factors evaluated were found to have relatively little influence on the measured NNPS. The beam spectrum, the use of the IEC apertures, the method of ROI normalization for regional exposure variation, and the ROI size all had  $\leq 2.3\%$  effect on the measured NNPS estimates, on average, across frequency. A factor that influenced the NNPS estimates in a slightly greater way, though still small, was the NPS analysis routine used. There was  $\leq 3.1\%$  difference on average, across frequency, between the three analysis routines. This difference was likely due to differences in ROI size and the width of the band of data in the two-dimensional NNPS averaged to yield the 1-D NNPS.

A factor that greatly influenced the very lowest spatial frequencies was the choice of detrending method used to correct for residual artifacts in the ROIs. It should be noted that while detrending introduces an element of arbitrariness to the determination of the NPS response, it does reduce the presence of low-frequency nonstochastic artifacts. The

second-order polynomial fit used by method B (in conjunction with  $128 \times 128$  ROIs) provided the best elimination of low-frequency artifacts. However, it is important to assess the prevalence of low-frequency artifacts for a given system, so it is recommended that a second analysis of the data be performed using a mean-image subtraction method on non-detrended data. By comparing the low-frequency NPS values with and without mean-image subtraction, one can ascertain the magnitude of any low-frequency artifacts.

All of the measured average relative differences between curves were found to be greater than the standard errors of the average, except for the differences due to directional dependence and method of regional exposure normalization. Thus, while most of the comparisons yielded differences that are likely statistically significant, for practical purposes, the absolute magnitude of differences was so small that the various methods can be considered roughly equivalent.

Methods A and B (including spectrum and analysis) agreed very well overall, differing by only  $\leq 0.8\%$  on average for frequencies above  $0.15 \text{ mm}^{-1}$ . The greatest difference between the two methods was at the very lowest frequencies, likely due to the difference in detrending methods. Thus, when comparing historical NPS data acquired and analyzed by these two methods, one would expect less than 1% error in the NNPS due to the method used.

Method C (including spectrum and analysis) agreed well with both methods A and B (0.9% difference, on average, between methods A and C above  $0.15 \text{ mm}^{-1}$  and  $\leq 1.6\%$  difference, on average, between methods B and C above  $0.15 \text{ mm}^{-1}$ ). Approximately the same trends were noted at the three exposure levels measured ( $E_{\text{nl}}/3.2$ ,  $E_{\text{nl}}$ , and  $3.2E_{\text{nl}}$ ). A factor of importance when making method C (IEC) measurements is that the high-purity Al filtration specified by the IEC ( $\geq 99.9\%$ ) has been associated with low-frequency artifacts, and thus we recommend the use of type 1100 Al (99.0% purity).<sup>26</sup>

While the current results indicate excellent agreement between the three methods evaluated, it should be noted that only a single detector was used for the comparative study. It is possible that other detectors would show a different relative performance from the three techniques. It is likely, though, that any differences in measured NNPS due to differences in the detector would be mostly due to the choice of beam spectrum and use of external apertures; other differences between methods are likely to have comparable magnitudes as those reported here. The quantitative use of the comparative findings need to be taken with additional precautions, as noted in the last paragraph of the Discussion in a concurrent paper.<sup>21</sup>

## VI. CONCLUSIONS

In summary, excellent agreement was found in NPS estimates obtained using methods A, B and C; historical comparisons between data reported on similar detectors using the three methods can be made with an overall disagreement of no more than about 1.6%. This finding suggests that any of the three methods, including the new IEC standard (method

C), can be used with confidence. We do, however, offer several recommendations based primarily on matters of practicality of the measurement procedures.

(1) The beam spectrum specified by IEC provides the most reliably calibrated spectrum. However, there was virtually no difference between the results measured with the three spectra reported here. As the IEC-specified spectrum is based on a measured HVL rather than a kilovoltage and filtration thickness, it is the least convenient to use because it requires a measurement to confirm target HVL.

(2) A ROI size of  $128 \times 128$  coupled with background detrending using a second-order polynomial fit yields the least susceptibility to residual shading artifacts at very low frequencies. Because the frequencies affected by residual shading are less than the lowest frequency specified by the IEC, one may ignore the detrending and use a ROI size of  $256 \times 256$  for purposes of measurement according to the IEC standard. For investigators interested in the noise performance at frequencies lower than those specified by the IEC, ROIs of size  $128 \times 128$  and second-order polynomial fit background detrending are recommended.

(3) The use of a subtraction method is recommended to further elucidate the degree of low-frequency residual artifacts.

(4) Frequency bins of  $0.05 \text{ mm}^{-1}$ , used by all three methods, give adequate resolution of the spectrum while providing reasonably smooth results.

(5) Overlapping of ROIs using the method specified by the IEC returned minimal benefit in improved precision of the NNPS estimate; the small improvement in measurement uncertainty was due to the slightly larger image area (hence, a slightly larger number of independent pixels) that could be placed within the collimated region of the beam when using overlapping ROIs of large size.

(6) Provided a constant number of independent image pixels is used for NPS analysis, the use of the IEC-specified beam-limiting apertures had little impact on the NPS estimate. Their use, however, severely limits the field of view, increases the number of images needed for a reasonably smooth NPS estimate, and complicates the image acquisition process. Their use, therefore, is not recommended.

## ACKNOWLEDGMENTS

The authors wish to thank Dr. Carl Ravin of the Duke Radiology Department for his assistance with this study. The flat-panel detector used for evaluation in this study was provided through a research agreement with GE Healthcare. This work was supported in part by grants from the National Institutes of Health (R01 CA80490 and R01 CA109074).

<sup>a</sup>This paper is part of a two-paper series. The readers are advised to also review the concurrent manuscript (Ref. 21).

<sup>1</sup>A. D. A. Maidment, M. Albert, P. C. Bunch, I. A. Cunningham, J. T. Dobbins III, R. M. Gagne, R. M. Nishikawa, R. F. Wagner, and R. L. Van Metter, "Standardization of NPS measurement: Interim report of AAPM TG16," *Proc. SPIE* **5030**, 523–532 (2003).

<sup>2</sup>"Medical electrical equipment—characteristics of digital x-ray imaging devices—part 1: determination of the detective quantum efficiency," International Electrotechnical Commission, Geneva, Switzerland, 2003.

<sup>3</sup>J. T. Dobbins III, D. L. Ergun, L. Rutz, D. A. Hinshaw, H. Blume, and D. C. Clark, "DQE(f) of four generations of computed radiography acquisition devices," *Med. Phys.* **22**, 1581–1593 (1995).

<sup>4</sup>E. Samei and M. J. Flynn, "Physical measures of image quality in photostimulable phosphor radiographic systems," *Proc. SPIE* **3032**, 328–338 (1997).

<sup>5</sup>E. Samei, R. S. Saunders, J. Y. Lo, J. T. Dobbins III, J. L. Jesneck, C. E. Floyd, Jr., and C. E. Ravin, "Fundamental imaging characteristics of a slot-scan digital chest radiographic system," *Med. Phys.* **31**, 2687–2698 (2004).

<sup>6</sup>C. D. Bradford, W. W. Peppler, and J. T. Dobbins III, "Performance characteristics of a Kodak computed radiography system," *Med. Phys.* **26**, 27–37 (1999).

<sup>7</sup>C. E. Floyd, Jr., R. J. Warp, J. T. Dobbins III, H. G. Chotas, A. H. Baydush, R. Vargas-Voracek, and C. E. Ravin, "Imaging characteristics of an amorphous silicon, flat-panel detector for digital chest radiography," *Radiology* **218**, 683–688 (2001).

<sup>8</sup>P. R. Granfors and R. Aufrichtig, "Performance of a  $41 \times 41\text{-cm}^2$  amorphous silicon flat panel x-ray detector for radiographic imaging applications," *Med. Phys.* **27**, 1324–1331 (2000).

<sup>9</sup>W. Hillen, U. Schiebel, and T. Zaengel, "Imaging performance of a digital storage phosphor system," *Med. Phys.* **14**, 744–751 (1987).

<sup>10</sup>M. J. Flynn and E. Samei, "Experimental comparison of noise and resolution for 2k and 4k storage phosphor radiography systems," *Med. Phys.* **26**, 1612–1623 (1999).

<sup>11</sup>W. Zhao, W. G. Ji, A. Debie, and J. A. Rowlands, "Imaging performance of amorphous selenium based flat-panel detectors for digital mammography: characterization of a small area prototype detector," *Med. Phys.* **30**, 254–263 (2003).

<sup>12</sup>J. H. Siewerdsen, L. E. Antonuk, Y. El-Mohri, J. Yorkston, and W. Huang, "Signal, noise power spectrum, and detective quantum efficiency of indirect-detection flat-panel imagers for diagnostic radiology," *Med. Phys.* **25**, 614–628 (1998).

<sup>13</sup>U. Neitzel, I. Maack, and S. Gunther-Kohfahl, "Image quality of a digital chest radiography system based on a selenium detector," *Med. Phys.* **21**, 509–516 (1994).

<sup>14</sup>E. Samei, "Image quality in two phosphor-based flat panel digital radiographic detectors," *Med. Phys.* **30**, 1747–1757 (2003).

<sup>15</sup>E. Samei and M. J. Flynn, "An experimental comparison of detector performance for computed radiography systems," *Med. Phys.* **29**, 447–459 (2002).

<sup>16</sup>E. Samei and M. J. Flynn, "An experimental comparison of detector performance for direct and indirect digital radiography systems," *Med. Phys.* **30**, 608–622 (2003).

<sup>17</sup>E. Samei, M. J. Flynn, H. G. Chotas, and J. T. Dobbins III, "DQE of direct and indirect digital radiography systems," *Proc. SPIE* **4320**, 189–197 (2001).

<sup>18</sup>K. A. Fetterly and N. J. Hangiandreou, "Effects of x-ray spectra on the DQE of a computed radiography system," *Med. Phys.* **28**, 241–249 (2001).

<sup>19</sup>S. M. Kengyelics, A. G. Davies, and A. R. Cowen, "A comparison of the physical imaging properties of Fuji ST-V, ST-VA, and ST-VN computed radiography image plates," *Med. Phys.* **25**, 2163–2169 (1998).

<sup>20</sup>J. T. Dobbins III, "Image quality metrics for digital systems," in *Handbook of Medical Imaging*, edited by R. L. van Metter, J. Beutel, and H. Kundel (Society of Photo-Optical Instrument Engineers, Bellingham, WA, 2000), Vol. 1, p. 161–222.

<sup>21</sup>E. Samei, J. T. Dobbins III, N. T. Ranger, and Y. Chen, "Inter-comparison of methods for image quality characterization: 1. modulation transfer function," *Med. Phys.* **33**, 1454–1465 (2006), preceding paper.

<sup>22</sup>J. C. Dainty and R. Shaw, *Image Science* (Academic, London, 1974).

<sup>23</sup>R. N. Bracewell, *The Fourier Transform and its Applications* (McGraw-Hill, New York, 1978).

<sup>24</sup>E. O. Brigham, *The Fast Fourier Transform* (Prentice-Hall, Englewood Cliffs, NJ, 1974).

<sup>25</sup>R. F. Wagner and J. M. Sandrik, "An introduction to digital noise analysis," in *The Physics of Medical Imaging: Recording System Measurements and Techniques*, edited by A. G. Haus (American Association of Physicists in Medicine, New York, 1979), pp. 524–545.

<sup>26</sup>N. T. Ranger, E. Samei, J. T. Dobbins III, and C. E. Ravin, "Measurement of the detective quantum efficiency in digital detectors consistent with the IEC 62220-1 standard: practical considerations regarding the choice of filter material," *Med. Phys.* **32**, 2305–2311 (2005).